Geometric phase induced interface states in mutually inverted two-dimensional photonic crystals

Xueqin Huang,[1] Yuting Yang,[2] Zhi Hong Hang,[2] Zhao-Qing Zhang,[1] and C. T. Chan[1,*]

[1]*Department of Physics and Institute for Advanced Study, Hong Kong University of Science and Technology, Clear Water Bay, Hong Kong, China*

[2]*College of Physics, Optoelectronics and Energy & Collaborative Innovation Center of Suzhou Nano Science and Technology, Soochow University, Suzhou 215006, China*

(Received 30 November 2015; revised manuscript received 18 January 2016; published 9 February 2016)

The exposed surface of a truncated photonic crystal (PC) may or may not carry surface states. Likewise, when two PCs are joined together, there is no assurance that interface states can be found at the boundary. We show, however, that interface states must exist at the boundary between a two-dimensional dielectric PC and its "inverted" partner (the conjugate structure formed by interchanging the high/low dielectric region) as long as a common gap can be found above the lowest band and the crystal structures possess a mirror symmetry on average along the interface direction. The interface states form deterministically as a result of different geometric phases of the bulk bands across the boundary. As the existence is protected by topological principles, the interface state will persist even in the limit of extremely small common gaps. The presence of interface states is demonstrated theoretically for a variety of PCs and also experimentally.

DOI: 10.1103/PhysRevB.93.085415

I. INTRODUCTION

The existence of interface/surface states in photonic crystals (PCs) were usually determined by numerical computations based on a cut and try approach [1–4]. It would be highly desirable if the conditions of their existence can be established on firm mathematical grounds. An analytical condition for interface/surface state formation in PCs does exist when the effective medium description is valid [5]. However, there is no general rule that can reliably predict the formation of interface states formed at the interface between two PCs. Recently, it has been shown that interface states can be found deterministically in two-dimensional (2D) dielectric PCs, which possess conical dispersions in the zone center, and the formation of the interface states can be traced to the presence of flat bands [6] specific to those systems. This is an example in which some simple rules can assure the existence of interface states, albeit for a fairly special class of PCs. Here we propose a simple method to create interface states in a large class of 2D PCs, and the condition holds as long as the two PCs on either side of the interface have mutually "inverted" structures (to be defined below) and there is a mirror symmetry on average along the interface direction. The interface state formation is related to the modern notion that the existence of surface/edge state is related to the bulk topological property of the **k**-space [7–26] where in this case it is governed by the geometric phases of the bands. Although the existence of interface states has been reported in a mutually inverted structure before [4], its physics origin has not established. We show here that there is a deep mathematical reason why the boundary state can form not just in some specific design, but in fact in a whole class of mutually inverted dielectric structures.

II. INTERFACE STATES IN SYSTEMS WITH C_{4v} SYMMETRY

Let us start by considering square lattice PCs shown schematically in Fig. 1(a). The PC1 is formed by dielectric cylinders (red color) with dielectric constant ε and radius r_d embedded in air. The PC2 is the inverted partner of PC1, formed by air cylinders (white color) with radius r_a embedded in a dielectric background with dielectric constant ε. The two PCs have the same lattice constant a. By tuning r_d or r_a, we can always align the first gaps above the lowest bands of these two mutually inverted structures so that they share a common gap in frequency. In Fig. 1(b), we plot the 2D bulk band structures for the transverse magnetic (TM) polarization with electric field along the cylinder axis for a pair of inverted structures where r_d or r_a are tuned to align the gaps ($\varepsilon = 11.9$, $r_d = 0.3a$, and $r_a = 0.45a$). A common gap exists in the frequency range between $0.193c/a$ and $0.261c/a$ along the ΓX direction. In Figs. 1(c) and 1(d), we consider the dispersions along k_x with a fixed $k_y = 0.2\pi/a$. It is crucial to point out here that the property of the lowest band gap (above the lowest allowed band) is dictated by Bragg scattering in the x direction. The structural variation in the y direction provides additional evanescent modes due to higher order diffractions along the y direction. In Appendix A, we show that the higher order diffraction modes have much shorter decay length than that due to the Bragg scattering and, therefore, have insignificant effects in the determination of interface state formation inside this gap. This allows us to consider a reduced one-dimensional (1D) system in which the material parameters are obtained by averaging the material parameters of the original 2D PCs along an orthogonal direction. Recently, it has been shown rigorously that in 1D PCs, the existence of an interface state inside a common gap is directly related to the topological properties of the bulk bands of the two constituent PCs [27]. The results have been successfully applied to the determination and observation of interface states in 1D PCs [28]. We want to emphasize that in general, 2D PCs cannot be reduced to equivalent 1D systems due to the existence of multiple interlayer diffraction channels. The surface impedance for 2D PCs is in general a tensorial quantity [29], and the edges of the band gap are not necessarily at the high symmetry points of the Brillouin zone. The relationship between the Zak phase and surface impedance that was established in 1D relies on a one-to-one correspondence between these quantities, but in

*Corresponding author: phchan@ust.hk

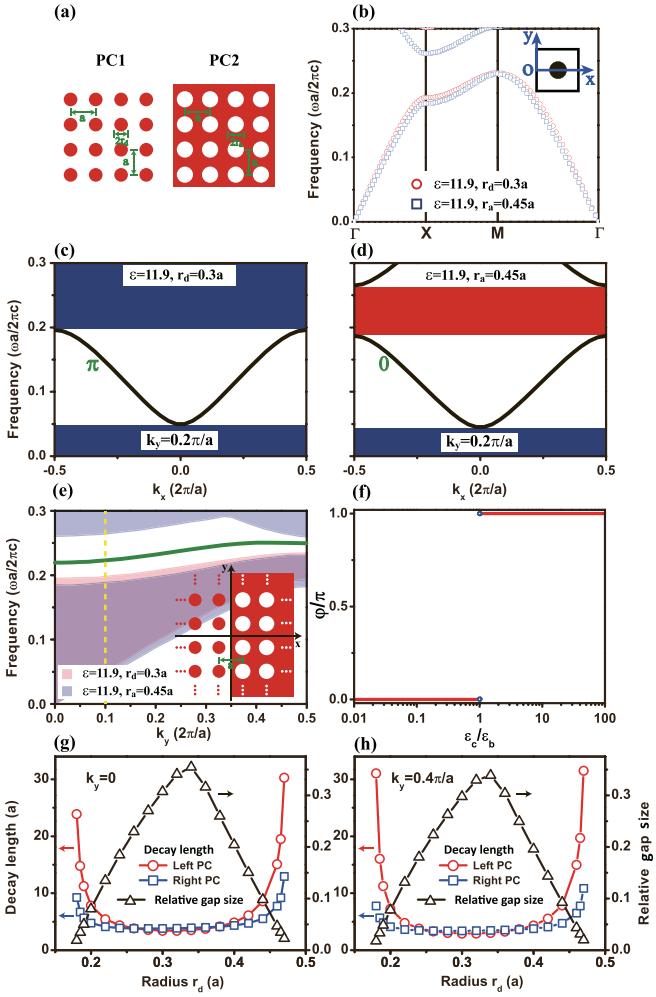

FIG. 1. (a) The schematic picture for the PC and its inverted partner. The PC1 consists of dielectric cylinders in air. The PC2 consists of air cylinders in a dielectric background. (b) The bulk band structures of the PCs: the red circles denote PC1 with $\varepsilon = 11.9$, $r_d = 0.3a$; blue squares denote PC2 with $\varepsilon = 11.9$, $r_a = 0.45a$. The inset shows the coordinate system for calculating the Zak phase. The reduced 1D bands with a fixed $k_y = 0.2\pi/a$ [yellow dashed line in (e)] are shown in (c) and (d) for PC1 and PC2, respectively. The Zak phases of the bulk bands are labeled with green color. The characters of the bulk gaps are labeled by the sign of Im(Z) with blue color for Im(Z) < 0 and red color for Im(Z) > 0. (e) Projected band structures along the k_y direction for PC1 (red) and PC2 (blue). The green line denotes interface states. (e) Inset: Schematic picture of an interface formed by two semi-infinite 2D PCs in a square lattice. (f) The Zak phase of the lowest band in a PC as a function of $\varepsilon_c/\varepsilon_b$. The PC consists of cylinders with relative permittivities ε_c and radii r_c in a square lattice embedded in a background with relative permittivity ε_b. Here, $r_c = 0.3a$. The relative gap sizes and the decay lengths of the interface states at $k_y = 0$ (g) and $k_y = 0.4\pi/a$ (h) as a function of the radius r_d in the left PC, respectively.

2D, such a correspondence cannot be found between the Zak phase (a scalar) and surface impedance (a tensor). However, we are going to demonstrate that under some conditions to be established below, 2D PCs can indeed be reduced to equivalent 1D systems.

We calculate the geometric Zak phases of the 1D bands shown in Figs. 1(c) and 1(d), and the results are used to label the bands. We note that the Zak phase depends on the choice of origin [30], and as such, only relative values are meaningful. Here, we choose the origin at the boundary of the unit cell, as shown in the inset of Fig. 1(b). This is a convenient choice because the surface impedance is measured at the boundary of the unit cell. We note that if other points are chosen to be the origin, the values of the Zak phases will change, but the difference of Zak phases will remain the same; it is the difference of Zak phases that matters. In Appendix B, we give two methods to calculate the Zak phases of the reduced 1D bulk bands depending on how to calculate the inner product and show that they give almost the same result. This is consistent with the assertion that the 2D gap interested here can be treated as a reduced 1D gap. We found that the lowest bands for PC1 and PC2 have Zak phases of π and 0, respectively. These results can also be obtained from the symmetries of two Bloch states at the two band edges [31] [see Appendix C]. The fact that the Zak phase changes from π to 0 in the lowest band as we invert the structure from dielectric cylinders to air holes can be understood physically as follows. For the lowest band, states near the zone center and at small $\mathbf{k}$ are well described by an effective homogenous medium; therefore, the characters of the states are more or less the same for PC1 and its inverted partner PC2. However, the structural variation in the x direction will determine the mode profile at the Brillion zone boundary $k_x = \pi/a$. The electromagnetic mode energy will concentrate in the high dielectric part and $|E_{n\vec{k}}(x,y)|$ will have different characters for PC1 and its conjugate PC2. As shown in Appendix C, after averaging over the y coordinate, $|\tilde{E}_{n,\vec{k}=(\pi/a,0.2\pi/a)}(x)|$ is peaked at the center of the unit cell for PC1 and at the boundary for PC2. The change of symmetry of the eigenmode of PC1 from $k_x = 0$ to $k_x = \pi/a$ gives it a Zak phase of π. It is known that in a system with inversion symmetry, if the center of the Wannier function coincides with the chosen origin, the Zak phase is zero; otherwise, it is π [32]. The lowest band in PC1 is a dielectric band, and hence the center of the Wannier function of this band coincides with the center of the cylinder. If the center of the cylinder was chosen as the origin, the Zak phase would have been zero. Since the origin was now chosen at the boundary of the unit cell, the Zak phase became π. This is consistent with that obtained from the symmetries of two Bloch states at the two band edges while PC2 has zero Zak phase, as shown in Appendix C. We note here that the change of the Zak phase from π to 0 in the lowest band as we invert the structure is very generic. The position of the high dielectric region and the low dielectric region relative to the inversion center of the system is the condition that determines the Zak phase in the low frequency band, and structural details are of secondary importance.

Let us now construct an interface as shown in the inset of Fig. 1(e), where a boundary along the y direction separates two semi-infinite PC1 and PC2. The corresponding projected band structures along the k_y direction are shown in Fig. 1(e). As the gaps are aligned, the projected band has a common band gap region. Accompanying the appearance of a common gap, a band of interface states (marked by a green line) appears. The existence of interface states is a direct consequence of the fact that the two constituent PCs have different Zak phases in the

reduced 1D bulk bands. Recently, the interface states arising from the Zak phases have been studied in experiments [24–26].

III. PHYSICAL ORIGIN OF THE INTERFACE STATE

To understand the topological origin of the interface state formation, we consider a particular interface state at frequency $0.23c/a$ with a fixed $k_y = 0.2\pi/a$, which is marked by the yellow dashed line in Fig. 1(e). The Bloch states along this vertical line represent the band states in the reduced 1D band structures along the k_x direction, as shown in Figs. 1(c) and 1(d). In 1D systems with inversion centers, the sign of the imaginary part of the surface impedance in a gap is related to the Zak phases of the bands below the gap [27,28]. Alternatively, the ratio of the signs of the imaginary parts of the surface impedances ($\mathrm{Im}(Z(\omega,k_y))$) in two adjacent gaps, say the nth and $(n-1)$th gaps, is related to the Zak phase (φ) of the band in between through a bulk-interface correspondence:

$$\mathrm{Sgn}[\mathrm{Im}[Z_n(\omega,k_y)]]/\mathrm{Sgn}[\mathrm{Im}[Z_{n-1}(\omega,k_y)]] = \exp[i(\varphi_{n-1}+\pi)]. \quad (1)$$

For the lowest gap in Figs. 1(c) and 1(d), it is easy to prove that the imaginary parts of the surface impedances of the two PCs are both negative, i.e., $\mathrm{Im}(Z(\omega,k_y)) < 0$ (marked in blue) [6]. Causality requires that $\mathrm{Re}(Z(\omega,k_y)) > 0$, and when we add an infinitesimally small loss to the PCs [33], we see that $\mathrm{Im}(Z(\omega,k_y)) < 0$. Using Eq. (1) and the Zak phases of the lowest bands, we found that $\mathrm{Im}(Z_L(\omega,k_y)) < 0$ in the second gap of PC1, while $\mathrm{Im}(Z_R(\omega,k_y)) > 0$ (marked in red) for PC2. Different signs of $\mathrm{Im}(Z_L(\omega,k_y))$ and $\mathrm{Im}(Z_R(\omega,k_y))$ imply that an interface state must exist at some frequency inside the second gap at which $\mathrm{Im}(Z_L(\omega,k_y)) + \mathrm{Im}(Z_R(\omega,k_y)) = 0$. This is because that the value of $\mathrm{Im}(Z(\omega,k_y))$ decreases monotonically from 0 to $-\infty$ and $+\infty$ to 0 with increasing frequency in a region with $\mathrm{Im}(Z(\omega,k_y)) < 0$ and $\mathrm{Im}(Z(\omega,k_y)) > 0$, respectively [27]. We note that the existence of a common band gap is a necessary but not sufficient condition for the existence of the interface states. What we have shown is that for mutually inverted structures, the interface states will form in the lowest gap due to the change of the bulk band Zak phase in the lowest band as we invert the structure across the interface.

In Fig. 1(f), we show the Zak phases of the lowest band in square lattice PCs [as those shown in Fig. 1(c) and Fig. 1(d)] for different values of the dielectric constant of the cylinder (ε_c) and those of the background (ε_b). We see that as long as the dielectric constant of the cylinder is larger than that of the background ($\varepsilon_c > \varepsilon_b$), the geometric phase is π, while it is zero if $\varepsilon_c < \varepsilon_b$. If we cross the boundary from a dielectric cylinder PC to its inverted partner, there must be a jump of the Zak phase of the lowest bulk band across the boundary, and this discontinuity gives rise to an interface state inside the common band gap above the first band. Figure 1(f) shows that this scenario is true not just for the $\varepsilon = 11.9$ chosen to compute the results of Fig. 1(e), but for any value of the dielectric constant. We also note that we found the same discontinuity shown in Fig. 1(f) for a large range of k_y, as it must be since the interface state cannot exist for just one particular value of k_y.

The geometric phase transition from left PC to right PC is effectively a topological transition. As the topological properties of the system will not change unless the gap is closed, the existence of interface states is assured no matter how tiny the common gap size is. The relationship between the gap size and the decay lengths of the interface states at two values of k_y ($k_y = 0$ and $0.4\pi/a$) illustrates this transition. In Figs. 1(g) and 1(h), we tune the relative gap size by varying the radius r_d of the cylinder in the left PC and keep the right PC unchanged. Here, the relative gap size is defined as the ratio between the gap size and the midgap frequency. As r_d is changed from $0.18a$ to $0.47a$, the relative gap size increases from zero to a large value and finally back to zero again, with a corresponding change of the decay length of the interface state. But irrespective of the size of the gap, there is always one band of interface state inside the gap. As long as the gap is there, the number of interface states cannot change. Only the decay length can change.

IV. MICROSTRUCTURES OF LOWER SYMMETRIES

In the above example, we have considered systems possessing C_{4v} symmetry. An example for the triangular lattice with C_{3v} symmetry is given in Appendix D. The high symmetries of the crystal structures ensure the existence of inversion centers in the corresponding reduced 1D structures, which in turn guarantees the existence of the interface states. Since the presence of inversion centers in the reduced 1D structures is the only requirement for the existence of interface states, we can lower the symmetry of the PCs in the search of interface states. The symmetry of a PC is not only determined by the lattice symmetry but also by the microstructures in a unit cell. Here, we first lower the symmetry of the microstructures in the unit cells of the PCs but keep the lattice structure unchanged. As an example, two PCs with two different microstructures are shown in Fig. 2(a). The top one (PC1) consists of a dielectric object (red color) with dielectric constant $\varepsilon = 11.9$ embedded in air (white color). The bottom one (PC2) is an inverted configuration two air holes (white color) embedded in an $\varepsilon = 11.9$ dielectric background (red color). Both unit cells possess only σ_x symmetry. There are two ways to construct an interface. One is shown in Fig. 2(b), in which the two semi-infinite PCs are arranged along the y direction so that both PCs have inversion centers in the reduced 1D structures. The projected band structures along the k_y direction are shown in Fig. 2(d). The filling ratio of the air holes in PC2 is purposely chosen so that PC1 and PC2 have a very small common gap in the projected band structures. A band of interface states marked by a green line is found inside the gap with a gap size to midgap ratio as small as 0.04, which can be seen from the inset of Fig. 2(f). Here we intentionally make the gap nearly closed in order to demonstrate the guaranteed existence of the interface states. In Figs. 2(f) and 2(g), the reduced 1D band structures with a fixed $k_y = 0.2\pi/a$ [labeled with yellow dashed line in Fig. 2(d)] for PC1 and PC2, respectively, are shown. The lowest bands of PC1 and PC2 have different Zak phases, which are π and 0, respectively. Based on the bulk-interface correspondence of Eq. (1), the surface impedances of PC1 and PC2 have different signs in the frequency range of the bulk gap above the lowest band, as labeled by different colors in

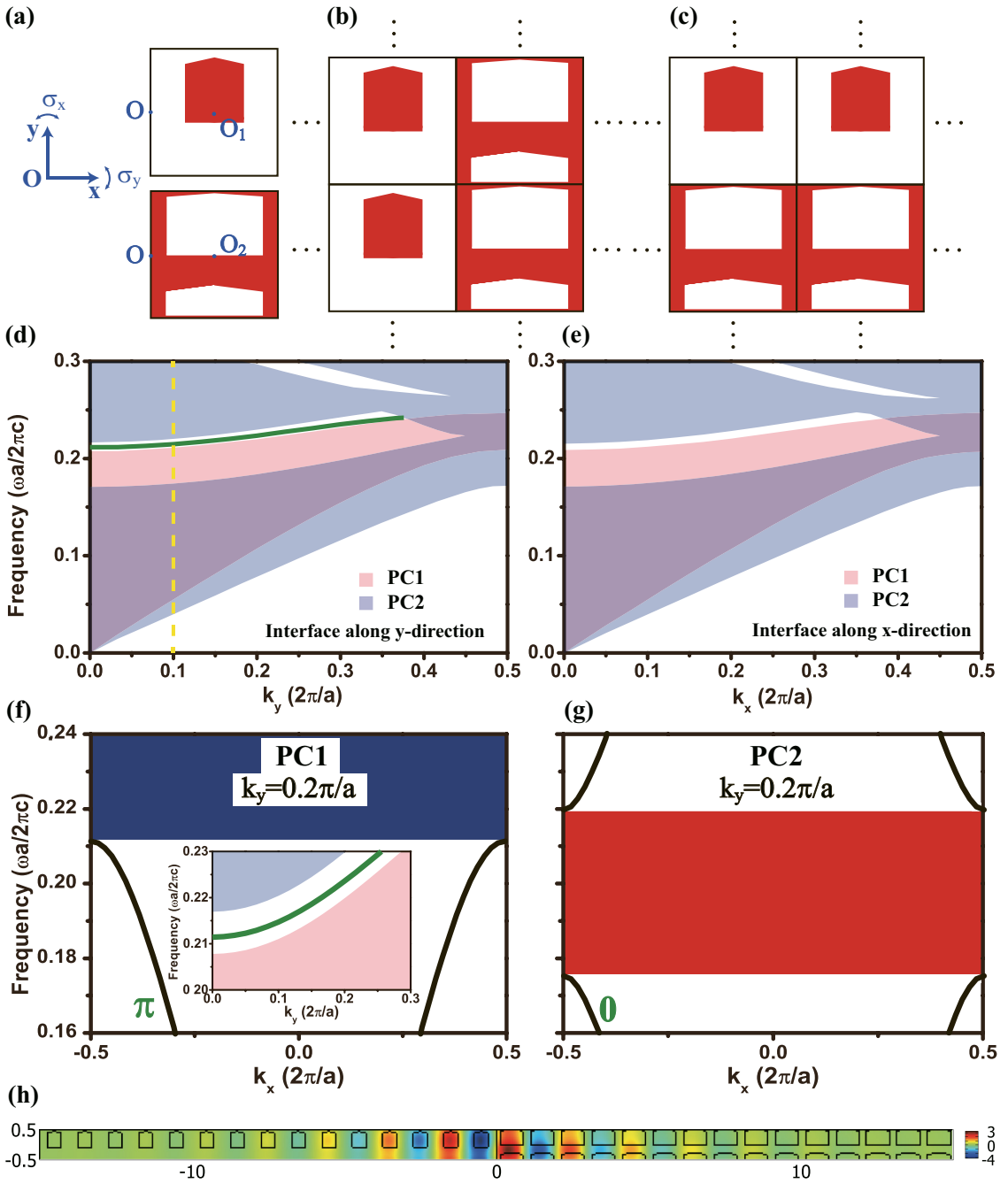

FIG. 2. (a) The unit cells of the PCs with red color denoting $\varepsilon = 11.9$ regions and white color denoting air. The top panel (PC1) consists of a dielectric object embedded in air, and the bottom panel (PC2) consists of two air objects embedded in dielectric. Both unit cells have mirror symmetry along only the y direction. The interfaces are constructed by joining the two PCs along the y direction (b) and x direction (c). Projected band structures of these two PCs are shown in (d) and (e) along the k_y and k_x directions, respectively, with red color denoting PC1 and blue color denoting PC2. The green line in (d) denotes interface states. There are no interface states at the interface shown in (e). The reduced 1D bands with a fixed $k_y = 0.2\pi/a$ [yellow dashed line in (d)] are shown in (f) and (g) for PC1 and PC2 in (b), respectively. (f) Inset: Enlarged projected bands of (d). The Zak phases of the bulk bands are labeled with green color. The characters of the bulk gaps are labeled by the sign of $\mathrm{Im}(Z)$ with blue color denoting $\mathrm{Im}(Z) < 0$ and red color denoting $\mathrm{Im}(Z) > 0$. (h) The eigenelectric field distribution of an interface state at $k_y = 0.2\,\pi/a$ along the x direction.

Figs. 1(f) and 1(g) [blue color for $\mathrm{Im}(Z) < 0$ and red color for $\mathrm{Im}(Z) > 0$]. An interface state must exist inside this gap as for the change of sign of the impedance across the interface, irrespective of the size of the gap. In Fig. 2(h), we show the electric field distribution of an interface state along the x direction at $k_y = 0.2\pi/a$. Localization of this state near the interface is clearly seen. However, if we arrange the two PCs along the x direction, as shown in Fig. 2(c), no interface states are found inside the gap, as shown in Fig. 2(e). This is due to the absence of reflection plane σ_y.

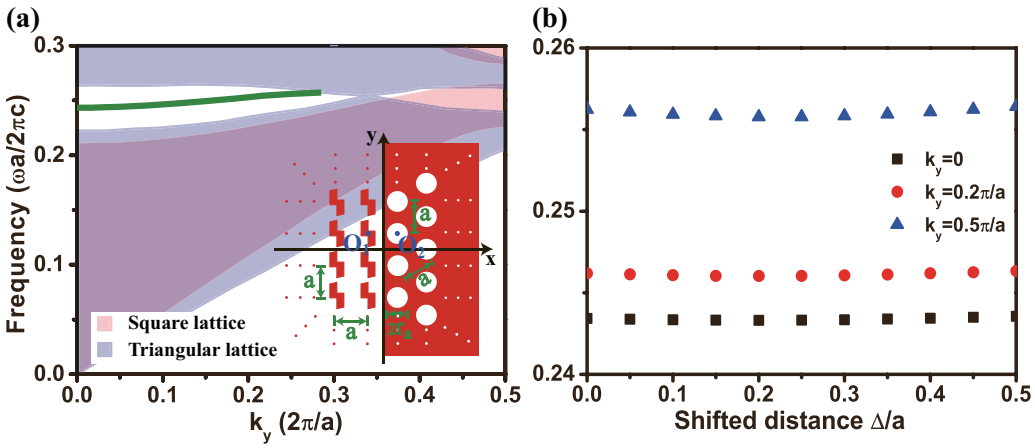

FIG. 3. (a) Projected band structures of these two PCs along the k_y direction for PC1 (red) and PC2 (blue). The green line is a band of the interface states. The inset shows the interface structure, with red color denoting high dielectrics and white color denoting air. PC1 consists of dielectric objects in a square lattice embedded in air, and PC2 consists of air cylinders in a triangular lattice embedded in a dielectric background. The distance between two nearest objects/cylinders is denoted by a for both PCs. (b) The eigenfrequency of an interface state at different k_y as a function of the relative shifted distance between the origins of two PCs. O_1 denotes the origin of PC1, and O_2 denotes that of PC2. Here, $\varepsilon = 11.9$, $r_d = 0.3a$, and $r_a = 0.42a$.

V. INTERFACE SEPARATING SYSTEMS WITH DIFFERENT LATTICE SYMMETRIES AND MICROSTRUCTURES

In Figs. 1(e) and 2(d), we demonstrated the existence of interface states using two PCs with the same lattice structure. Now we consider inverted configurations with different lattice symmetries. An example is shown in the inset of Fig. 3(a), in which PC1 consists of dielectric objects in a square lattice embedded in air and PC2 is formed by air cylinders in a triangular lattice embedded in a dielectric background. Since the presence of inversion centers in the reduced 1D PC is the only requirement for interface state formation, the mirror symmetry in the microstructures shown in previous examples was also relaxed. For instance, the object in the PC1 now consists of one half of the unit cell of PC1 in Fig. 2(a) and its inversion symmetric part. The PC1 now does not even possess σ_x symmetry. The presence of inversion centers is recovered only after taking the average of dielectric constant along the y direction. In this case, the two PCs are different not only in the symmetries of the microstructures but also lattice symmetries. The projected band structures of the two PCs as well as a band of interface states are shown in Fig. 3(a). We then shift the two PCs along the y direction with a relative distance $\Delta = O_1 - O_2$, where O_1 and O_2 are the origins of PC1 and PC2. The frequencies of interface states for several values of k_y as Δ changes are plotted in Fig. 3(b). The frequency of the interface state at a certain k_y is almost independent of Δ. This shows that a mirror symmetry on average along the interface direction is sufficient to guarantee the existence of interface states. In Appendix E, we demonstrate the existence of interface states in two mutually inverted PCs in an oblique lattice. In this structure, the presence of inversion centers normal to the interface is a result of parameter averaging along the interface direction.

VI. EXPERIMENTAL VERIFICATION OF THE INTERFACE STATES

The existence of the interface states at the boundary of mutually inverted structures is also verified by microwave experiments. The experimental setup is shown in Fig. 4(a). Two PCs with mutually inverted structures were assembled in the xy plane inside a parallel-plate waveguide composed by two flat aluminum plates. PC1 consists of a square array of alumina rods with $\varepsilon_d = 8.5$, $r_d = 3.75$ mm embedded in air. Its inverted partner PC2 consists of a square array of air holes with $r_a = 5$ mm embedded in glass background with $\varepsilon_b = 3.75$. The lattice constants of both PCs are $a = 12.4$ mm. The height of the alumina rods and the glass slab are 11 mm. The separation between the two aluminum plates is set as 12 mm, which is slightly larger than the height of the rods and the slab but smaller than half the wavelength in interest ($\sim$20 mm for 7$\sim$8 GHz where interface states were observed) to ensure that the whole experimental chamber can only support transverse electromagnetic modes. The PC arrays were fixed to the lower aluminum plate. The PCs are surrounded by absorbing materials (in blue) to avoid unwanted scattering. The projected band structures along k_y direction are shown in Fig. 4(b). The green line denotes a band of interface states found by numerical simulations. A time-harmonic monopole antenna is located at the position marked by the red arrow. As the frequencies under investigation are inside the common gap for both PCs, evanescent wave is used to excite interface states. The lower aluminum plate along with the whole experimental setup was mounted on a translational stage in the xy plane, and thus the electric field distribution of the whole sample can be recorded via a field-scanning antenna fixed in a hole in the upper aluminum plate (not shown). A microwave vector network analyzer (Agilent E5071C) is used as both source and recorder of microwave signals. The measured interface states at different k_y are shown by the blue triangles and

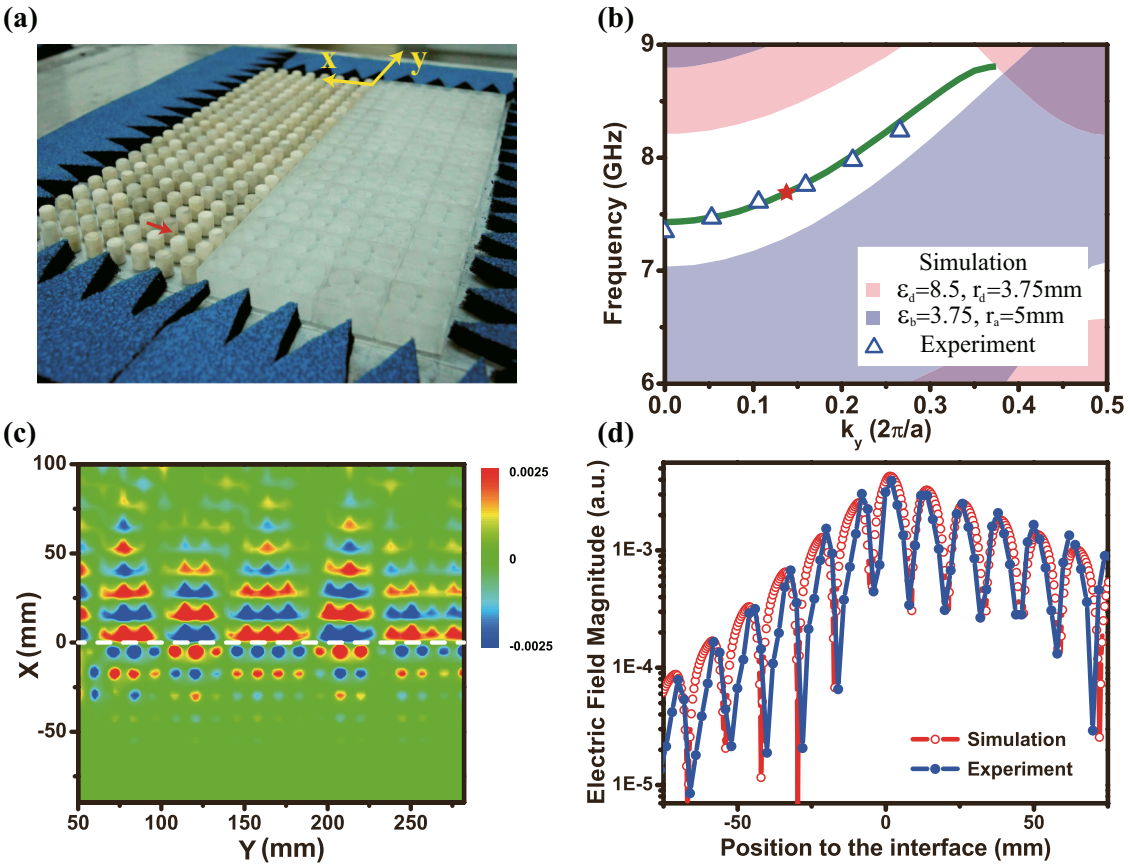

FIG. 4. (a) The photo of the experimental setup. The structural parameters are given in the text. The red arrow marks the position of the point source. (b) Projected band structures for PC1 (red) and PC2 (blue). The green line marks the calculated interface states. The blue triangles are measured by the experiment. (c) The electric field distribution of the interface state at $f = 7.67$ GHz [marked by a red star in (b)]. The interface is at the origin of the x axis ($x = 0$). (d) Comparing calculated and measured averaged electric field magnitude in the direction normal to the interface.

agree perfectly with the simulations. Figure 4(c) shows the measured electric field distribution of the interface state at the frequency $f = 7.67$ GHz [marked by a red star in Fig. 4(b)]. In Fig. 4(d), we plot the averaged electric field magnitude along the direction perpendicular to the interface for this state. The averaged electric field magnitude is obtained by averaging the electric field magnitude in the unit cell at $y \sim 175$ mm. The red hollow circles denote the simulation results, and the blue dots denote the measured results. It is clearly seen that the electric field amplitude decays exponentially away from the interface with decay lengths of 40.4 mm and 92.3 mm for PC1 and PC2, respectively. Again, the experiment is in good agreement with the simulation.

VII. CONCLUSION

In summary, we showed that interface states can be found at the boundary that separates a 2D dielectric PC and its inverted partner. A dielectric crystal is typically made by embedding a periodic array of objects with a high dielectric constant (e.g., Si cylinders) in a background of low dielectric constant (e.g., air). Its inverted partner is a conjugate structure in which the high and low dielectric components switch position. The existence of the interface state is due to the abrupt change of the surface impedance of the PC across the interface in the first band gap, and this change in surface impedance can be traced to the fact that the geometric phases of the lowest band of a dielectric PC and its inverted partner generally have different values. This principle is illustrated with many examples. This paradigm can also be used to create interface states in 2D phononic crystals.

Finally, we note that the discontinuous jump of geometric phase across the boundary guarantees the existence of the boundary mode. There is no mechanism within this principle that dictates the transport properties of the state. If we want to realize topologically protected one-way transport, we can add additional mechanisms, such as time reversal breaking or spin-momentum locking mechanisms to the PC [7–23] at the expense of more complexity in structure and constituent material (e.g., Yttrium iron garnet) and external field.

ACKNOWLEDGMENTS

We thank Dr. M. Xiao for stimulating discussions. This paper is supported by Research Grants Council, Hong Kong (Project No. AoE/P-02/12). Experimental work in Soochow University is supported by National Natural Science Foundation of China (No. 11304215 and No. 11574226), Natural Science Foundation of Jiangsu Province (No. BK20130281), and a Project Funded by the Priority Academic Program Development of Jiangsu Higher Education Institutions (PAPD).

APPENDIX A: THE GAP PROPERTY OF A 2D PC IN THE FIRST GAP ABOVE THE LOWEST BAND

For an interface along the y direction shown in the inset of Fig. 1(e), we want to show that for the first gap above the lowest band shown in Figs. 1(c) or 1(d), the gap property is dictated by the Bragg scattering in the x direction. The effects due to higher order diffractions along the y direction are insignificant in the determination of interface states. The Maxwell equation for a 2D PC in the TM polarization with the electric field E out of the 2D plane (the xy plane) is

$$\frac{1}{\varepsilon(\vec{r})}\left[\frac{\partial^2}{\partial x^2}+\frac{\partial^2}{\partial y^2}\right]E(\vec{r})=\frac{\omega^2}{c^2}E(\vec{r}). \tag{A1}$$

Here, $\varepsilon(\vec{r})$ is the position-dependent relative permittivity, ω is the angular frequency, and c is the speed of light in vacuum. By using plane wave expansion, we write

$$\frac{1}{\varepsilon(\vec{r})}=\sum_{\vec{G}}\kappa(\vec{G})e^{i\vec{G}\cdot\vec{r}}, \tag{A2}$$

$$E(\vec{r})=E_{n\vec{k}}(\vec{r})=\sum_{\vec{G}}E_{n\vec{k}}(\vec{G})e^{i(\vec{k}+\vec{G})\cdot\vec{r}}, \tag{A3}$$

where $E_{n\vec{k}}$ denotes the Bloch state with wave vector $\vec{k}$ in the nth band and $\vec{G}$ is the reciprocal lattice vector. For a square lattice with a lattice constant a, $\vec{G}=G_{x,n}\hat{i}+G_{y,m}\hat{j}=\frac{2\pi}{a}(n\hat{i}+m\hat{j})$ (m,n are integers). Substituting Eqs. (A2) and (A3) into Eq. (A1), we obtain

$$\sum_{\vec{G}'}\kappa(\vec{G}-\vec{G}')|\vec{k}+\vec{G}'|^2E_{n\vec{k}}(\vec{G}')=\frac{\omega^2_{n\vec{k}}}{c^2}E_{n\vec{k}}(\vec{G}). \tag{A4}$$

The band structure of the PC is determined by the following secular equation:

$$\mathrm{Det}\left[\sum_{\vec{G}'}\kappa(\vec{G}-\vec{G}')|\vec{k}+\vec{G}'|^2-\frac{\omega^2_{n\vec{k}}}{c^2}\delta_{\vec{G},\vec{G}'}\right]=0. \tag{A5}$$

For an interface state with a fixed k_y inside a gap, k_x becomes a complex number. The imaginary part of k_x gives the decay length of the state along the x direction. To find the complex solutions of k_x at a given frequency ω inside the gap, we need to solve Eq. (A5) in the following form:

$$\mathrm{Det}\left[k_x^2\sum_{\vec{G}'}\kappa(\vec{G}-\vec{G}')+2k_x\sum_{\vec{G}'}\kappa(\vec{G}-\vec{G}')G'_x+\sum_{\vec{G}'}\kappa(\vec{G}-\vec{G}')\left[G'^2_x+(k_y+G'_y)^2\right]-\frac{\omega^2}{c^2}\delta_{\vec{G},\vec{G}'}\right]=0. \tag{A6}$$

As Eq. (A6) involves a matrix of infinite dimensions, some truncation is necessary in actual calculations. Since we are only interested in the first gap above the lowest band, we consider only the $n,m=0,\pm1$ components of $\vec{G}$, i.e.,$G_{x,1}=G_{y,1}=-G_{x,-1}=-G_{y,-1}=\frac{2\pi}{a}$ and $G_{x,0}=G_{y,0}=0$. For simplicity, we set $k_y=0$. Equation (A6) then reduces to the following form:

$$\mathrm{Det}\begin{pmatrix}
\kappa_{00}\left[(k_x+G_{x,-1})^2+G_{y,-1}^2\right]-\frac{\omega^2}{c^2} & \kappa_{-1,0}\left[k_x^2+G_{y,-1}^2\right] & \kappa_{-2,0}\left[(k_x+G_{x,1})^2+G_{y,-1}^2\right] & \kappa_{0,-1}(k_x+G_{x,-1})^2 & \kappa_{-1,-1}k_x^2 & \kappa_{-2,-1}(k_x+G_{x,1})^2 & \kappa_{0,-2}\left[(k_x+G_{x,-1})^2+G_{y,1}^2\right] & \kappa_{-1,-2}\left[k_x^2+G_{y,1}^2\right] & \kappa_{-2,-2}\left[(k_x+G_{x,1})^2+G_{y,1}^2\right]\\
\kappa_{1,0}\left[(k_x+G_{x,-1})^2+G_{y,-1}^2\right] & \kappa_{00}\left[k_x^2+G_{y,-1}^2\right]-\frac{\omega^2}{c^2} & \kappa_{-1,0}\left[(k_x+G_{x,1})^2+G_{y,-1}^2\right] & \kappa_{1,-1}(k_x+G_{x,-1})^2 & \kappa_{0,-1}k_x^2 & \kappa_{-1,-1}(k_x+G_{x,1})^2 & \kappa_{1,-2}\left[(k_x+G_{x,-1})^2+G_{y,1}^2\right] & \kappa_{0,-2}\left[k_x^2+G_{y,1}^2\right] & \kappa_{-1,-2}\left[(k_x+G_{x,1})^2+G_{y,1}^2\right]\\
\kappa_{2,0}\left[(k_x+G_{x,-1})^2+G_{y,-1}^2\right] & \kappa_{1,0}\left[k_x^2+G_{y,-1}^2\right] & \kappa_{00}\left[(k_x+G_{x,1})^2+G_{y,-1}^2\right]-\frac{\omega^2}{c^2} & \kappa_{2,-1}(k_x+G_{x,-1})^2 & \kappa_{1,-1}k_x^2 & \kappa_{0,-1}(k_x+G_{x,1})^2 & \kappa_{2,-2}\left[(k_x+G_{x,-1})^2+G_{y,1}^2\right] & \kappa_{1,-2}\left[k_x^2+G_{y,1}^2\right] & \kappa_{0,-2}\left[(k_x+G_{x,1})^2+G_{y,1}^2\right]\\
\kappa_{0,1}\left[(k_x+G_{x,-1})^2+G_{y,-1}^2\right] & \kappa_{-1,1}\left[k_x^2+G_{y,-1}^2\right] & \kappa_{-2,1}\left[(k_x+G_{x,1})^2+G_{y,-1}^2\right] & \kappa_{00}(k_x+G_{x,-1})^2-\frac{\omega^2}{c^2} & \kappa_{-1,0}k_x^2 & \kappa_{-2,0}(k_x+G_{x,1})^2 & \kappa_{0,-1}\left[(k_x+G_{x,-1})^2+G_{y,1}^2\right] & \kappa_{-1,-1}\left[k_x^2+G_{y,1}^2\right] & \kappa_{-2,-1}\left[(k_x+G_{x,1})^2+G_{y,1}^2\right]\\
\kappa_{1,1}\left[(k_x+G_{x,-1})^2+G_{y,-1}^2\right] & \kappa_{0,1}\left[k_x^2+G_{y,-1}^2\right] & \kappa_{-1,1}\left[(k_x+G_{x,1})^2+G_{y,-1}^2\right] & \kappa_{1,0}(k_x+G_{x,-1})^2 & \kappa_{00}k_x^2-\frac{\omega^2}{c^2} & \kappa_{-1,0}(k_x+G_{x,1})^2 & \kappa_{1,-1}\left[(k_x+G_{x,-1})^2+G_{y,1}^2\right] & \kappa_{0,-1}\left[k_x^2+G_{y,1}^2\right] & \kappa_{-1,-1}\left[(k_x+G_{x,1})^2+G_{y,1}^2\right]\\
\kappa_{2,1}\left[(k_x+G_{x,-1})^2+G_{y,-1}^2\right] & \kappa_{1,1}\left[k_x^2+G_{y,-1}^2\right] & \kappa_{0,1}\left[(k_x+G_{x,1})^2+G_{y,-1}^2\right] & \kappa_{2,0}(k_x+G_{x,-1})^2 & \kappa_{1,0}k_x^2 & \kappa_{00}(k_x+G_{x,1})^2-\frac{\omega^2}{c^2} & \kappa_{2,-1}\left[(k_x+G_{x,-1})^2+G_{y,1}^2\right] & \kappa_{1,-1}\left[k_x^2+G_{y,1}^2\right] & \kappa_{0,-1}\left[(k_x+G_{x,1})^2+G_{y,1}^2\right]\\
\kappa_{0,2}\left[(k_x+G_{x,-1})^2+G_{y,-1}^2\right] & \kappa_{-1,2}\left[k_x^2+G_{y,-1}^2\right] & \kappa_{-2,2}\left[(k_x+G_{x,1})^2+G_{y,-1}^2\right] & \kappa_{0,1}(k_x+G_{x,-1})^2 & \kappa_{-1,1}k_x^2 & \kappa_{-2,1}(k_x+G_{x,1})^2 & \kappa_{00}\left[(k_x+G_{x,-1})^2+G_{y,1}^2\right]-\frac{\omega^2}{c^2} & \kappa_{-1,0}\left[k_x^2+G_{y,1}^2\right] & \kappa_{-2,0}\left[(k_x+G_{x,1})^2+G_{y,1}^2\right]\\
\kappa_{1,2}\left[(k_x+G_{x,-1})^2+G_{y,-1}^2\right] & \kappa_{0,2}\left[k_x^2+G_{y,-1}^2\right] & \kappa_{-1,2}\left[(k_x+G_{x,1})^2+G_{y,-1}^2\right] & \kappa_{1,1}(k_x+G_{x,-1})^2 & \kappa_{0,1}k_x^2 & \kappa_{-1,1}(k_x+G_{x,1})^2 & \kappa_{1,0}\left[(k_x+G_{x,-1})^2+G_{y,1}^2\right] & \kappa_{00}\left[k_x^2+G_{y,1}^2\right]-\frac{\omega^2}{c^2} & \kappa_{-1,0}\left[(k_x+G_{x,1})^2+G_{y,1}^2\right]\\
\kappa_{2,2}\left[(k_x+G_{x,-1})^2+G_{y,-1}^2\right] & \kappa_{1,2}\left[k_x^2+G_{y,-1}^2\right] & \kappa_{0,2}\left[(k_x+G_{x,1})^2+G_{y,-1}^2\right] & \kappa_{2,1}(k_x+G_{x,-1})^2 & \kappa_{1,1}k_x^2 & \kappa_{0,1}(k_x+G_{x,1})^2 & \kappa_{2,0}\left[(k_x+G_{x,-1})^2+G_{y,1}^2\right] & \kappa_{1,0}\left[k_x^2+G_{y,1}^2\right] & \kappa_{00}\left[(k_x+G_{x,1})^2+G_{y,1}^2\right]-\frac{\omega^2}{c^2}
\end{pmatrix}=0 \tag{A7}$$

where $\kappa_{m,n}$ denotes $\kappa(G_{x,m},G_{y,n})$, $\vec{k}=(k_x,0)$.

To obtain the gap property from Eq. (A7), it is useful to consider first the limit of a homogenous medium with all the off-diagonal terms in Eq. (A7) being small. In this limit, the zeroth order solutions of k_x are determined by the diagonal elements

of the three block matrices shown in Eq. (A7), i.e.,

$$\frac{\omega^2}{c^2} = \kappa_{00}(k_x + G_{x,-1})^2, \quad \frac{\omega^2}{c^2} = \kappa_{00}k_x^2, \quad \frac{\omega^2}{c^2} = \kappa_{00}(k_x + G_{x,1})^2, \tag{A8}$$

for the middle block, and

$$\frac{\omega^2}{c^2} = \kappa_{00}\left[(k_x + G_{x,-1})^2 + G_{y,-1}^2\right], \quad \frac{\omega^2}{c^2} = \kappa_{00}\left[k_x^2 + G_{y,-1}^2\right], \quad \frac{\omega^2}{c^2} = \kappa_{00}\left[(k_x + G_{x,1})^2 + G_{y,-1}^2\right], \tag{A9}$$

and

$$\frac{\omega^2}{c^2} = \kappa_{00}\left[(k_x + G_{x,-1})^2 + G_{y,1}^2\right], \quad \frac{\omega^2}{c^2} = \kappa_{00}\left[k_x^2 + G_{y,1}^2\right], \quad \frac{\omega^2}{c^2} = \kappa_{00}\left[(k_x + G_{x,1})^2 + G_{y,1}^2\right], \tag{A10}$$

for the upper and lower blocks, respectively.

In Eq. (A8), there are six solutions for k_x at a given frequency, i.e., $k_x = \pm\frac{\omega}{\sqrt{\kappa_{00}}c} - G_{x,-1}$, $k_x = \pm\frac{\omega}{\sqrt{\kappa_{00}}c}$, and $k_x = \pm\frac{\omega}{\sqrt{\kappa_{00}}c} - G_{x,1}$. At the reduced Brillouin zone boundary with $k_x = \pm\frac{G_{x,1}}{2}$, the middle equation gives $\omega_b = \frac{\sqrt{\kappa_{00}}G_{x,1}c}{2}$. At this frequency, it is easy to see that the first and third equations give the solutions of $k_x = \frac{G_{x,1}}{2}$ and $k_x = -\frac{G_{x,1}}{2}$, respectively, due to the periodicity of the band structure. Before we introduce the scattering terms, $\kappa_{m,n}(m,n \neq 0)$, we should point out that Eqs. (A9) or (A10) gives two evanescent solutions of k_x at ω_b, i.e.,

$$\mathrm{Re}(k_x) = 0 \quad \text{and} \quad \mathrm{Im}(k_x) = \pm\sqrt{G_{y,\pm1}^2 - \frac{G_{x,1}^2}{4}} \tag{A11}$$

in the reduced zone. It will be shown later that these solutions represent the leading terms in solutions of k_x with $\mathrm{Re}(k_x) = 0$ when $\kappa_{m,n}(m,n \neq 0)$.

When the Bragg scatterings along the x direction are introduced, i.e., $\kappa_{\pm1,0} \neq 0$, a gap will open along the ΓX direction. Since this gap hosts the interface states shown in Fig. 1, we are interested in finding the properties of this gap and the effects due to higher order diffractions in the y direction. In the following, we focus our discussions on the complex solutions of k_x at the midgap frequency ω_b. Since we are interested in the first gap above the lowest band, we consider complex solutions of k_x due to the nonzero terms $\kappa_{\pm1,0}$ and $\kappa_{0,\pm1}$ only. Equation (A7) is now simplified to

$$\mathrm{Det}\begin{bmatrix}
\left[(k_x+G_{x,-1})^2+G_{y,-1}^2\right]-\frac{\omega_{nk}^2}{\kappa_{00}c^2} & \frac{\kappa_{-1,0}}{\kappa_{00}}\left[k_x^2+G_{y,-1}^2\right] & 0 \\
\frac{\kappa_{1,0}}{\kappa_{00}}\left[(k_x+G_{x,-1})^2+G_{y,-1}^2\right] & \left[k_x^2+G_{y,-1}^2\right]-\frac{\omega_{nk}^2}{\kappa_{00}c^2} & \frac{\kappa_{-1,0}}{\kappa_{00}}\left[(k_x+G_{x,1})^2+G_{y,-1}^2\right] \\
0 & \frac{\kappa_{1,0}}{\kappa_{00}}\left[k_x^2+G_{y,-1}^2\right] & \left[(k_x+G_{x,1})^2+G_{y,-1}^2\right]-\frac{\omega_{nk}^2}{\kappa_{00}c^2}
\end{bmatrix}
\begin{bmatrix}
\frac{\kappa_{0,-1}}{\kappa_{00}}(k_x+G_{x,-1})^2 & 0 & 0 \\
0 & \frac{\kappa_{0,-1}}{\kappa_{00}}k_x^2 & 0 \\
0 & 0 & \frac{\kappa_{0,-1}}{\kappa_{00}}(k_x+G_{x,1})^2
\end{bmatrix}
\begin{bmatrix}
0 & 0 & 0 \\
0 & 0 & 0 \\
0 & 0 & 0
\end{bmatrix}$$

$$\begin{bmatrix}
\frac{\kappa_{0,1}}{\kappa_{00}}\left[(k_x+G_{x,-1})^2+G_{y,-1}^2\right] & 0 & 0 \\
0 & \frac{\kappa_{0,1}}{\kappa_{00}}\left[k_x^2+G_{y,-1}^2\right] & 0 \\
0 & 0 & \frac{\kappa_{0,1}}{\kappa_{00}}\left[(k_x+G_{x,1})^2+G_{y,-1}^2\right]
\end{bmatrix}
\begin{bmatrix}
(k_x+G_{x,-1})^2-\frac{\omega_{nk}^2}{\kappa_{00}c^2} & \frac{\kappa_{-1,0}}{\kappa_{00}}k_x^2 & 0 \\
\frac{\kappa_{1,0}}{\kappa_{00}}(k_x+G_{x,-1})^2 & k_x^2-\frac{\omega_{nk}^2}{\kappa_{00}c^2} & \frac{\kappa_{-1,0}}{\kappa_{00}}(k_x+G_{x,1})^2 \\
0 & \frac{\kappa_{1,0}}{\kappa_{00}}k_x^2 & (k_x+G_{x,1})^2-\frac{\omega_{nk}^2}{\kappa_{00}c^2}
\end{bmatrix}
\begin{bmatrix}
\frac{\kappa_{0,-1}}{\kappa_{00}}\left[(k_x+G_{x,-1})^2+G_{y,1}^2\right] & 0 & 0 \\
0 & \frac{\kappa_{0,-1}}{\kappa_{00}}\left[k_x^2+G_{y,1}^2\right] & 0 \\
0 & 0 & \frac{\kappa_{0,-1}}{\kappa_{00}}\left[k_x^2+G_{y,1}^2\right]
\end{bmatrix}$$

$$\begin{bmatrix}
\frac{\kappa_{0,1}}{\kappa_{00}}(k_x+G_{x,-1})^2 & 0 & 0 \\
0 & \frac{\kappa_{0,1}}{\kappa_{00}}k_x^2 & 0 \\
0 & 0 & \frac{\kappa_{0,1}}{\kappa_{00}}(k_x+G_{x,1})^2
\end{bmatrix}
\begin{bmatrix}
0 & 0 & 0 \\
0 & 0 & 0 \\
0 & 0 & 0
\end{bmatrix}
\begin{bmatrix}
\left[(k_x+G_{x,-1})^2+G_{y,1}^2\right]-\frac{\omega_{nk}^2}{\kappa_{00}c^2} & \frac{\kappa_{-1,0}}{\kappa_{00}}\left[k_x^2+G_{y,1}^2\right] & 0 \\
\frac{\kappa_{1,0}}{\kappa_{00}}\left[(k_x+G_{x,-1})^2+G_{y,1}^2\right] & \left[k_x^2+G_{y,1}^2\right]-\frac{\omega_{nk}^2}{\kappa_{00}c^2} & \frac{\kappa_{-1,0}}{\kappa_{00}}\left[k_x^2+G_{y,1}^2\right] \\
0 & \frac{\kappa_{1,0}}{\kappa_{00}}\left[k_x^2+G_{y,1}^2\right] & \left[(k_x+G_{x,1})^2+G_{y,1}^2\right]-\frac{\omega_{nk}^2}{\kappa_{00}c^2}
\end{bmatrix} = 0 \tag{A12}$$

The three 3×3 block matrices in the diagonal entries (surrounded by rectangles) involve the terms $G_{y,-1}$, $G_{y,0}$, and $G_{y,1}$, respectively. Each of these block matrices describes the interactions between $G_{x,\pm1}$ and $G_{x,0}$ through $\kappa_{\pm1,0}$ with a fixed $G_{y,n}(n = 0, \pm 1)$. The off-diagonal block matrices denote interactions between $G_{y,\pm1}$ and $G_{y,0}$ through $\kappa_{0,\pm1}$.

Since the middle block matrix involves only the Bragg scattering along the x direction, we first solve this middle block matrix. From the determinant of the middle block matrix, we find the following solutions of k_x in the reduced Brillouin zone at ω_b:

$$k_x \approx \pm\frac{G_{x,1}}{2} \pm i\frac{G_{x,1}}{4}\frac{\kappa_{1,0}}{\kappa_{00}}. \tag{A13}$$

Equation (A13) shows that $\kappa_{1,0}$ open a gap at the reduced Brillouin zone boundary and the decay length at ω_b is inversely proportional to $\frac{\kappa_{1,0}}{\kappa_{00}}$. The presence of nonzero $\kappa_{0,\pm1}$ is expected to modify $\mathrm{Im}(k_x)$ in Eq. (A13) as well as the $\mathrm{Im}(k_x)$ of the evanescent modes with $\mathrm{Re}(k_x) = 0$. We solve Eq. (A12) analytically at ω_b and find the following solutions of k_x in the reduced

Brillouin zone:

$$k_x \approx \pm\frac{G_{x,1}}{2} \pm i\left(\frac{G_{x,1}}{4}\frac{\kappa_{1,0}}{\kappa_{00}} + \frac{G_{x,1}\left(35G_{x,1}^2+76G_{y,1}^2\right)}{128G_{y,1}^2}\frac{\kappa_{1,0}}{\kappa_{00}}\left(\frac{\kappa_{0,1}}{\kappa_{00}}\right)^2\right) \tag{A14}$$

and

$$k_x \approx \pm i\left(\sqrt{G_{y,1}^2-\frac{G_{x,1}^2}{4}} + \frac{G_{x,1}^2\left(G_{x,1}^2+16G_{y,1}^2\right)}{64G_{y,1}^2\sqrt{G_{y,1}^2-\frac{G_{x,1}^2}{4}}}\left(\frac{\kappa_{1,0}}{\kappa_{00}}\right)^2 + \frac{G_{x,1}^2\sqrt{G_{y,1}^2-\frac{G_{x,1}^2}{4}}}{4G_{y,1}^2}\left(\frac{\kappa_{0,1}}{\kappa_{00}}\right)^2\right). \tag{A15}$$

From Eq. (A14), we find a correction term to the $\mathrm{Im}(k_x)$ of Eq. (A13), which is about a factor $(\frac{\kappa_{0,1}}{\kappa_{00}})^2$ smaller than the $\mathrm{Im}(k_x)$ term due to Bragg scatterings. For the evanescent modes at $\mathrm{Re}(k_x)=0$, there are two corrections in the $\mathrm{Im}(k_x)$ in Eq. (A15); each has a factor $(\frac{\kappa_{1,0}}{\kappa_{00}})^2$ or $(\frac{\kappa_{0,1}}{\kappa_{00}})^2$ smaller than the leading term in Eq. (A11). For instance, using the parameters shown in Fig. 1, we obtain $\frac{\kappa_{1,0}}{\kappa_{00}} = \frac{\kappa_{0,1}}{\kappa_{00}} \approx -0.22$ for the left PC and $\frac{\kappa_{1,0}}{\kappa_{00}} = \frac{\kappa_{0,1}}{\kappa_{00}} \approx 0.25$ for the right PC. Thus, the decaying lengths of the evanescent modes inside the gap are mainly determined by the $\mathrm{Im}(k_x)$ in Eqs. (A11) and (A13). Furthermore, since $\mathrm{Im}(k_x)$ in Eq. (A13) or Eq. (A14) is much smaller than that in Eq. (A11) or Eq. (A15), the decay modes caused by higher order diffractions $G_{y,\pm1}$ have much smaller decay length than that caused by the Bragg scattering $G_{x,\pm1}$. Using Eqs. (A14) and (A15), we find that the ratio of $\mathrm{Im}(k_x)$ in Eq. (A14) and Eq. (A15) is 1/13 for the left PC and 1/11 for the right PC. Thus, we can safely conclude that the interface states is primarily governed by the 1D Bragg scattering in the x direction. It should be mentioned the dielectric contrast adopted in Fig. 1 is $\varepsilon_{\mathrm{dielectric}} = 11.9$ and $\varepsilon_{\mathrm{air}} = 1$. A smaller contrast makes the ratio of $\mathrm{Im}(k_x)$ even smaller as the dominant term in Eq. (A15) is independent of the scattering parameters.

APPENDIX B: THE CALCULATION OF THE ZAK PHASES OF THE REDUCED 1D BULK BANDS USING TWO DIFFERENT METHODS

In the previous discussions, we have shown that the property of the band gap above the lowest band in a 2D PC can be treated as that of a reduced 1D PC. Using the eigenfields of the 2D PC, we calculate the Zak phases of the reduced 1D bulk bands. There are two ways to calculate the Zak phase of the reduced 1D bulk bands depending on how we calculate the inner product. One is to obtain the reduced 1D eigenfields and then perform the inner product, the other is to directly use the 2D eigenfields to perform the inner product. We will find that these two methods give almost the same result. This is consistent with the assertion that the 2D gap interested here can be treated as a reduced 1D gap.

In the first method, we calculate the Zak phases of the reduced 1D bulk bands using the formula $\tilde{\varphi}_n = i\int_{-\pi/a}^{\pi/a}\langle\tilde{u}_{nk_x}(x)|\tilde{\varepsilon}(x)\partial_{k_x}|\tilde{u}_{nk_x}(x)\rangle dk_x$ [32]. Here, $\tilde{u}_{nk_x}(x)$ is the cell periodic part of the Bloch function of the $\tilde{E}_{nk_x}(x)$ field for the nth reduced 1D band at a particular k_x, i.e., $\tilde{u}_{nk_x}(x) = e^{-ik_x x}\tilde{E}_{nk_x}(x)$. The electric field $\tilde{E}_{nk_x}(x)$ in the reduced 1D case is obtained by integrating the electric field $E_{n\vec{k}}(x,y)$ in 2D case along the y direction, i.e., $\tilde{E}_{nk_x}(x) = \frac{1}{a}\int_0^a E_{nk_x,k_y=k_{||}}(x,y)e^{-ik_y y}dy$. The $\tilde{\varepsilon}(x)$ is the position-dependent relative permittivity of the reduced 1D system, i.e., $\tilde{\varepsilon}(x) = \frac{1}{a}\int_0^a \varepsilon(x,y)dy$. In the numerical calculations, the integral formula is implemented as a summation, then the integral domain for k_x is segmented into M discrete points. Each point is denoted by $k_{x,l}$ with $l = 1,\cdots,M$. For simplicity, $k_{x,l}$ in the subscript will be replaced by l. So $\tilde{\varphi}_n = -\sum_{l=1}^{M}\mathrm{Im}\ln\tilde{\phi}_{n,l} = -\sum_{l=1}^{M}\mathrm{Im}\ln\langle\tilde{u}_{n,l}(x)|\tilde{\varepsilon}(x)|\tilde{u}_{n,l+1}(x)\rangle$ in the limit of large M [30]. The inner product becomes

$$\begin{aligned}\tilde{\phi}_{n,l} &= \langle\tilde{u}_{n,l}(x)|\tilde{\varepsilon}(x)|\tilde{u}_{n,l+1}(x)\rangle \\ &= \int_{\text{unit cell}}\tilde{\varepsilon}(x)\tilde{u}_{n,l}^*(x)\cdot\tilde{u}_{n,l+1}(x)dx. \end{aligned}\tag{B1}$$

Substituting $\varepsilon(\vec{r}) = \sum_{\vec{G}}\eta(\vec{G})e^{i\vec{G}\cdot\vec{r}}$ and Eq. (A3) into Eq. (B1), we can obtain

$$\begin{aligned}\tilde{\phi}_{n,l} &= \frac{1}{a^3}\int_{\text{unit cell}}\sum_{\vec{G},\vec{G}',\vec{G}''}\int_0^a \eta(\vec{G})e^{i\vec{G}\cdot\vec{r}}dy \\ &\quad\cdot\int_0^a E_{z,n,l,k_y=k_{||}}^*(\vec{G}')e^{-i\vec{G}'\cdot\vec{r}'}dy' \\ &\quad\cdot\int_0^a E_{z,n,l+1,k_y=k_{||}}(\vec{G}'')e^{i\vec{G}''\cdot\vec{r}''}dy''dx \\ &= \frac{1}{a^3}\int_{\text{unit cell}}\sum_{\vec{G},\vec{G}',\vec{G}''}\iiint\eta(\vec{G})\cdot E_{z,n,l,k_y=k_{||}}^*(\vec{G}') \\ &\quad\cdot E_{z,n,l+1,k_y=k_{||}}(\vec{G}'')e^{i(G_y y-G'_y y'+G''_y y'')}dydy'dy'' \\ &\quad\times e^{i(G_x-G'_x+G''_x)x}dx. \end{aligned}\tag{B2}$$

Here, we use the numerical package COMSOL to calculate the eigenmodes $E_{nk_x,k_y=k_{||}}(x,y)$ (normalized by the electric energy) of 2D PC for different k_x and a fixed $k_y = k_{||}$. The periodic gauge $\tilde{u}_{n,-\pi/a}(x) = e^{i2\pi x/a}\tilde{u}_{n,\pi/a}(x)$ is applied at two ends.

In the second method, we calculate the Zak phases of the reduced 1D bulk bands using the formula $\varphi_n = i\int_{-\pi/a}^{\pi/a}\langle u_{nk_x,k_y=k_{||}}|\varepsilon(\vec{r})\partial_{k_x}|u_{nk_x,k_y=k_{||}}\rangle dk_x$ [32], where $u_{n\vec{k}}$ is the cell periodic part of the Bloch function of the $E_{n\vec{k}}(\vec{r})$ field for the nth band at a particular $\vec{k}$ and $\varepsilon(\vec{r})$ is position-dependent relative permittivity. In the numerical calculations, the integral formula is also implemented as a summation, so $\varphi_n = -\sum_{l=1}^{M}\mathrm{Im}\ln\phi_{n,l} = -\sum_{l=1}^{M}\mathrm{Im}\ln\langle u_{n,l,k_y=k_{||}}|\varepsilon(\vec{r})|u_{n,l+1,k_y=k_{||}}\rangle$ in the limit of large M [30]. The inner product becomes

$$\begin{aligned}\phi_{n,l} &= \langle u_{n,l,k_y=k_{||}}|\varepsilon(\vec{r})|u_{n,l+1,k_y=k_{||}}\rangle \\ &= \iint_{\text{unit cell}}\varepsilon(\vec{r})u_{n,l,k_y=k_{||}}^*(\vec{r})\cdot u_{n,l+1,k_y=k_{||}}(\vec{r})d\vec{r}. \end{aligned}\tag{B3}$$

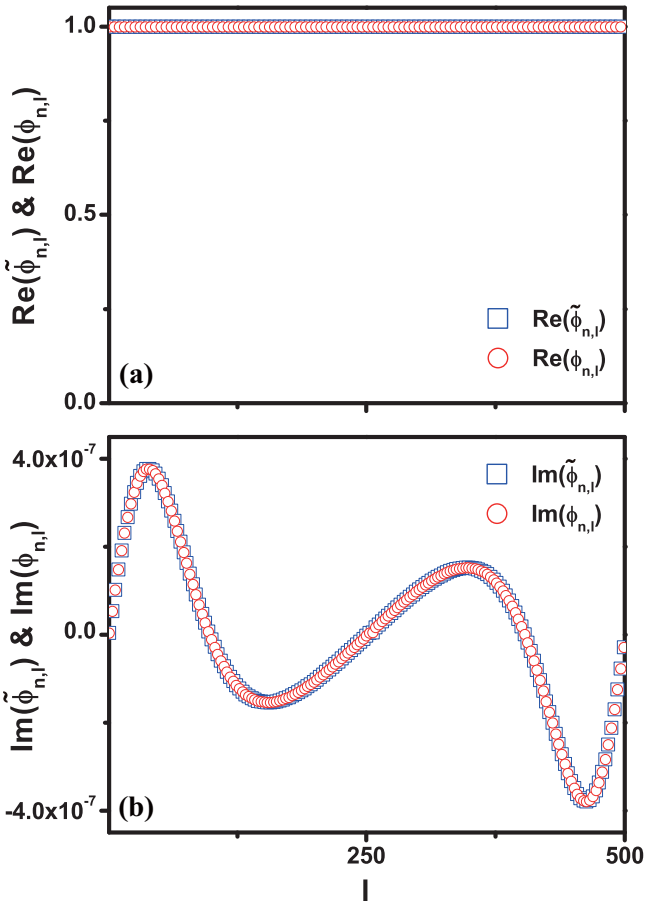

FIG. 5. The calculation of the Zak phases of the reduced 1D bulk bands with two different methods. The PC consists of dielectric cylinders with $\varepsilon = 11.9$, $r_d = 0.3a$ in air. (a) Real parts of $\tilde{\phi}_{n,l}$ and $\phi_{n,l}$ as a function of l. (b) Imaginary parts of $\tilde{\phi}_{n,l}$ and $\phi_{n,l}$ as a function of l. Blue squares denote $\tilde{\phi}_{n,l}$, and red circles denote $\phi_{n,l}$.

Fourier transform $\varepsilon(\vec{r}) = \sum_{\vec{G}} \eta(\vec{G}) e^{i\vec{G}\cdot\vec{r}}$ and substituting Eq. (A3) into Eq. (B3),

$$\phi_{n,l} = \iint_{\text{unit cell}} \sum_{\vec{G},\vec{G}',\vec{G}''} \eta(\vec{G}) E^{*}_{z,n,l,k_y=k_{||}}(\vec{G}') \cdot E_{z,n,l+1,k_y=k_{||}}(\vec{G}'') e^{i(\vec{G}-\vec{G}'+\vec{G}'')\cdot\vec{r}} d\vec{r}. \quad \text{(B4)}$$

The eigenmodes of $E_{n\vec{k}}$ (normalized by the electric energy) and $u_{n\vec{k}}$ are related by $E_{n\vec{k}}(\vec{r}) = u_{n\vec{k}}(\vec{r}) e^{i\vec{k}\cdot\vec{r}}$. To obtain the Zak phases of these bands, we use the numerical package COMSOL to calculate the eigenmodes $u_{nk_x,k_y=k_{||}}(\vec{r})$ of 2D PC for different k_x and a fixed $k_y = k_{||}$. The periodic gauge $u_{n,-\pi/a,k_y}(x,y) = e^{i2\pi x/a} u_{n,\pi/a,k_y}(x,y)$ is applied at two ends. In this paper, we choose the origin at the left boundary of the unit cell labeled as O shown in the inset of Figs. 1(b) and 2(a) for both the first and second methods. Comparing Eqs. (B2) with (B4), it is easily seen that if Eq. (B2) is equivalent to Eq. (B4), it implies that $G_y = G'_y = G''_y = 0$. Figure 5 shows the calculated phases $\phi_{n,l}$ and $\tilde{\phi}_{n,l}$ as a function of l. The excellent agreement between these two functions shows again that the 2D system can be considered as a reduced 1D case.

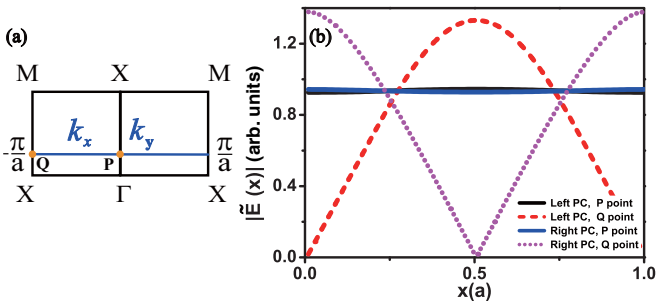

FIG. 6. (a) The diagram shows the 2D Brillouin zone in a square lattice. The blue line denotes the reduced 1D Brillouin zone along k_x direction for a fixed $k_y = 0.2\pi/a$. The **k**-points at P and Q are located at the center and the boundary of the reduced 1D Brillouin zone, respectively. (b) The absolute value of the electric field $|\tilde{E}(x)|$ as a function of x. Black solid and red dashed lines represent $|\tilde{E}(x)|$ at P and Q points for the left PC, respectively. Blue solid and purple dotted lines represent $|\tilde{E}(x)|$ at P and Q points for the right PC, respectively. Here, the left PC is dielectric cylinders with $\varepsilon = 11.9$ and radii $r_d = 0.3a$ embedded in air. The right PC is air cylinders with radii $r_a = 0.45a$ embedded in a dielectric background with $\varepsilon = 11.9$. Both the lattice constants of the two PCs are a.

APPENDIX C: THE ZAK PHASE OF THE REDUCED 1D BAND

The reduced 1D Brillouin zone is shown by a blue line in Fig. 6(a). In addition to a brute force integration in k-space along the band, the Zak phase can also be determined by the symmetry of Bloch states at two high symmetry points of the reduced 1D Brillouin zone [31], which are labeled by P ($k_x = 0, k_y$) and Q ($k_x = -\pi/a, k_y$) in Fig. 6(a). To obtain the equivalent electric field $\tilde{E}_{nk_x}(x)$ of the nth band in the reduced 1D case, we integrate the electric field $E_{n\vec{k}}(x,y)$ in 2D along the y direction, i.e., $\tilde{E}_{nk_x}(x) = \frac{1}{a}\int_0^a E_{n\vec{k}}(x,y) e^{-ik_y y} dy$. Kohn's results [31] can be generalized to the EM wave such that if either $|\tilde{E}_P(x=0)| = |\tilde{E}_Q(x=0)| = 0$ or $|\tilde{E}_P(x=0)| \neq 0$ and $|\tilde{E}_Q(x=0)| \neq 0$, the Zak phase is 0; otherwise it is π. In Fig. 6(b), we plot $\tilde{E}_{nk_x}(x)$ for the two PCs at P and Q points in one unit cell. Here, the left PC is dielectric cylinders with $\varepsilon = 11.9$ and radii $r_d = 0.3a$ embedded in air. The right PC is air cylinders with radii $r_a = 0.45a$ embedded in a dielectric background with $\varepsilon = 11.9$. At $x = 0$ point, we find $|\tilde{E}_P(x=0)| \neq 0$ and $|\tilde{E}_Q(x=0)| = 0$ for the left PC; therefore, the Zak phase is π. Whereas for the right PC, $|\tilde{E}_P(x=0)| \neq 0$ and $|\tilde{E}_Q(x=0)| \neq 0$; therefore, the Zak phase is 0.

APPENDIX D: THE INTERFACE STATES IN TWO PCS IN A TRIANGULAR LATTICE

In this section, we show the interface states at the interface formed by two PCs in a triangular lattice shown in the inset of Fig. 7(b). The left PC consists of dielectric cylinders with relative permittivities ε and radii r_d in air. The inverted PC on the right is formed by air cylinders with radii r_a in a dielectric background with relative permittivity ε. The distance between the two nearest cylinders is denoted by a for both PCs.

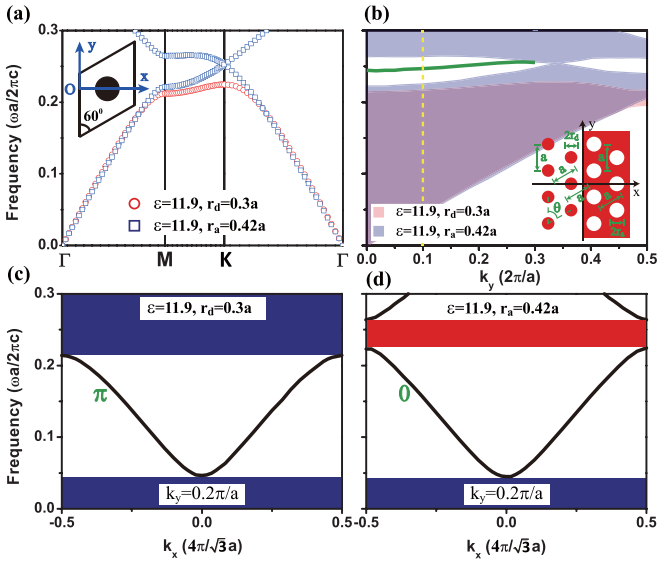

FIG. 7. (a) The bulk band structures of two PCs: red circles denote the dielectric cylinders with $\varepsilon = 11.9$, $r_d = 0.3a$ in air (left PC); blue squares denote air cylinders with $r_a = 0.42a$ in a dielectric background with $\varepsilon = 11.9$ (right PC). The inset shows the coordinate for calculating the Zak phase. (b) The projected band structures of these two PCs along the k_y direction with red color denoting the left PC and blue color denoting the right PC. The green line denotes a band of the interface states. (b) Inset: Schematic picture of an interface constructed by two semi-infinite 2D PCs in a triangular lattice. The reduced 1D bands with a fixed $k_y = 0.2\pi/a$ [yellow dashed line in (b)] are shown in (c) and (d) for the left and right PCs, respectively. The Zak phases of the bulk bands are labeled with green color. The characters of the bulk gaps are labeled by the sign of $\mathrm{Im}(Z)$ with blue color for $\mathrm{Im}(Z) < 0$ and red color for $\mathrm{Im}(Z) > 0$.

Figure 7(a) shows the bulk band structures of the two PCs with $\varepsilon = 11.9$, $r_d = 0.3a$, and $r_a = 0.42a$. The corresponding projected band structures along the k_y direction are shown in Fig. 7(b). The green line inside the common gap denotes a band of interface states. To interpret the existence of interface states, we evaluate the Zak phases of the two lowest bands of the reduced 1D band structures shown in Figs. 7(c) and 7(d) for a particular value of $k_y = 0.2\pi/a$, as indicated by the yellow dashed line in Fig. 7(b). The results are π and 0 for the left and right PCs, respectively. According to the bulk-interface correspondence of Eq. (1), the signs of the surface impedances in the common gap of the two PCs are opposite, which in turn guarantees the existence of an interface state inside this gap.

APPENDIX E: THE INTERFACE STATES IN TWO PCS IN AN OBLIQUE LATTICE

In this section, we show the existence of interface states in two PCs in an oblique lattice. The schematic diagram of the interface is similar to the case of the triangular lattice with $\theta = 60^\circ$, as shown in the inset of Fig. 7(b). Here, we study an oblique lattice with $\theta = 70^\circ$. The projected band structures of two constituent PCs are shown in Fig. 8(a). The relative permittivity and radius of the cylinder in the left PC are $\varepsilon = 11.9$ and $r_d = 0.3a$, respectively. The radius of the air cylinder and the relative permittivity of the background in the right PC are $r_a = 0.33a$ and $\varepsilon = 11.9$, respectively. A band of interface states exists in a very small common gap above the lowest band shown as a green line in Fig. 8(a). To see clearly the interface states in the projected band structures, an enlarged figure is shown in the inset of Fig. 8(b). To investigate the existence of interface states, we plot the reduced 1D band structures with a fixed $k_y = 0$, as shown in Figs. 8(b) and 8(c). The Zak phases of the lowest bands of the left and right PCs are π and 0, respectively. The origin for the calculation of the Zak phase is chosen at Point O shown in the inset of Fig. 8(a). Using the bulk-interface correspondence of Eq. (1), the signs of $\mathrm{Im}(Z)$ in the common gaps of the two PCs are opposite. This guarantees the existence of an interface state inside this gap.

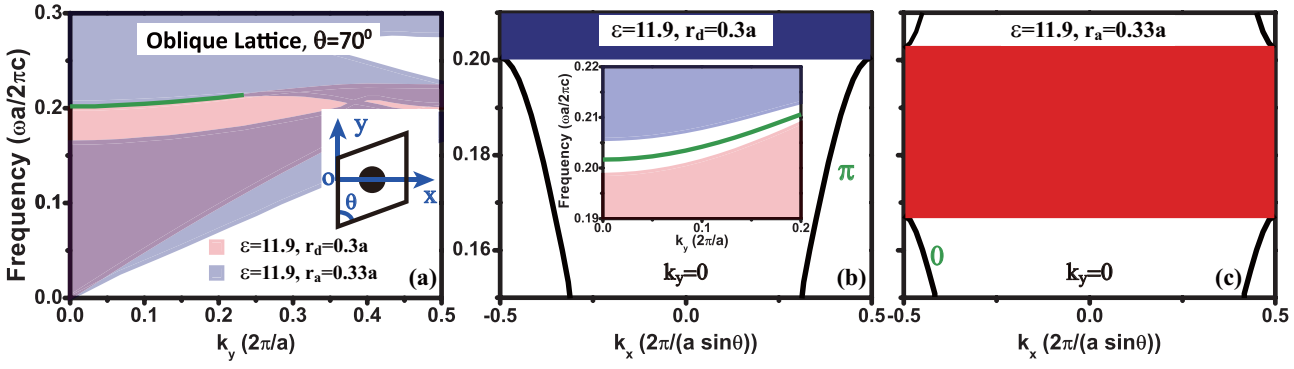

FIG. 8. (a) The projected band structures of two PCs in an oblique lattice with $\theta = 70^\circ$ along the k_y direction, one with dielectric cylinders in air (red color, left PC) and the other with air cylinders in a dielectric background (blue color, right PC). The relative permittivities of dielectric cylinders and dielectric background are $\varepsilon = 11.9$. The radii of the dielectric cylinders and air cylinders are $r_d = 0.3a$ and $r_a = 0.33a$, respectively. The green line denotes a band of the interface states. The inset shows the coordinate for calculating the Zak phase. The reduced 1D bands with a fixed $k_y = 0$ are shown in (b) and (c) for the left and right PCs, respectively. (b) Inset: Enlarged projected bands of (a). The Zak phases of the bulk bands are labeled with green color. The characters of the bulk gaps are labeled by the sign of $\mathrm{Im}(Z)$ with blue color for $\mathrm{Im}(Z) < 0$ and red color for $\mathrm{Im}(Z) > 0$.

[1] J. D. Joannopoulos, S. G. Johnson, J. N. Winn, and R. D. Meade, *Photonic Crystals: Molding the Flow of Light*, 2nd ed. (Princeton University Press, Princeton, NJ, 2008).
[2] L. L. Lin and Z. Y. Li, Phys. Rev. B **63**, 033310 (2001).
[3] Y. S. Zhou, B. Y. Gu, and F. H. Wang, J. Phys.: Condens. Matter **15**, 4109 (2003).
[4] M. Mehrabi, A. Soltani-Vala, and J. Barvestani, Opt. Commun. **284**, 5444 (2011).
[5] Y. Wu, J. Li, Z. Q. Zhang, and C. T. Chan, Phys. Rev. B **74**, 085111 (2006).
[6] X. Huang, M. Xiao, Z. Q. Zhang, and C. T. Chan, Phys. Rev. B **90**, 075423 (2014).
[7] S. Raghu and F. D. M. Haldane, Phys. Rev. A **78**, 033834 (2008).
[8] F. D. M. Haldane and S. Raghu, Phys. Rev. Lett. **100**, 013904 (2008).
[9] Z. Wang, Y. D. Chong, J. D. Joannopoulos, and M. Soljacic, Phys. Rev. Lett. **100**, 013905 (2008).
[10] Z. Yu, G. Veronis, Z. Wang, and S. Fan, Phys. Rev. Lett. **100**, 023902 (2008).
[11] Z. Wang, Y. Chong, J. D. Joannopoulos, and M. Soljacic, Nature **461**, 772 (2009).
[12] K. Fang, Z. Yu, and S. Fan, Nat. Photon. **6**, 782 (2012).
[13] M. Hafezi, E. A. Demler, M. D. Lukin, and J. M. Taylor, Nat. Phys. **7**, 907 (2011).
[14] M. Hafezi, S. Mittal, J. Fan, A. Migdall, and J. M. Taylor, Nat. Photon. **7**, 1001 (2013).
[15] Y. E. Kraus, Y. Lahini, Z. Ringel, M. Verbin, and O. Zilberberg, Phys. Rev. Lett. **109**, 106402 (2012).
[16] M. C. Rechtsman, J. M. Zeuner, Y. Plotnik, Y. Lumer, D. Podolsky, F. Dreisow, S. Nolte, M. Segev, and A. Szameit, Nature **496**, 196 (2013).
[17] A. B. Khanikaev, S. H. Mousavi, W. K. Tse, M. Kargarian, A. H. MacDonald, and G. Shvets, Nat. Mater. **12**, 233 (2013).
[18] L. Lu, L. Fu, J. D. Joannopoulos, and M. Soljacic, Nat. Photon. **7**, 294 (2013).
[19] Y. Plotnik, M. C. Rechtsman, D. Song, M. Heinrich, J. M. Zeuner, S. Nolte, Y. Lumer, N. Malkova, J. Xu, A. Szameit, Z. Chen, and M. Segev, Nature Mater. **13**, 57 (2014).
[20] G. Q. Liang and Y. D. Chong, Phys. Rev. Lett. **110**, 203904 (2013).
[21] L. Lu, J. D. Joannopoulos, and M. Soljacic, Nat. Photon. **8**, 821 (2014).
[22] A. A. Skirlo, L. Lu, and M. Soljacic, Phys. Rev. Lett. **113**, 113904 (2014).
[23] W. J. Chen, S. J. Jiang, X. D. Chen, B. Zhu, L. Zhou, J. W. Dong, and C. T. Chan, Nat. Common. **5**, 5782 (2014).
[24] N. Malkova, I. Hromada, X. Wang, G. Bryant, and Z. Chen, Opt. Lett. **34**, 1633 (2009).
[25] M. C. Rechtsman, Y. Plotnik, J. M. Zeuner, D. Song, Z. Chen, A. Szameit, and M. Segev, Phys. Rev. Lett. **111**, 103901 (2013).
[26] C. Poli, M. Bellec, U. Kuhl, F. Mortessagne, and H. Schomerus, Nat. Common. **6**, 6710 (2015).
[27] M. Xiao, Z. Q. Zhang, and C. T. Chan, Phys. Rev. X **4**, 021017 (2014).
[28] M. Xiao, G. Ma, Z. Y. Yang, P. Shen, Z. Q. Zhang, and C. T. Chan, Nat. Phys. **11**, 240 (2015).
[29] F. J. Lawrence, L. C. Botten, K. B. Dossou, C. M. Sterke, and R. C. Mcphedran, Phys. Rev. A **80**, 023826 (2009).
[30] R. Resta, J. Phys.: Condens. Matter **12**, R107 (2000).
[31] W. Kohn, Phys. Rev. **115**, 809 (1959).
[32] J. Zak, Phys. Rev. Lett. **62**, 2747 (1989).
[33] M. Xiao, Bulk and surface correspondence through geometric phases in classical wave systems. Ph.D. thesis, Hong Kong University of Science and Technology, 2014.